Carbon Dioxide Capture for Storage in Deep Geologic Formations – Results from the CO_2 Capture Project

Geologic Storage of Carbon Dioxide with Monitoring and Verification

Volume 2

Elsevier Internet Homepage – http://www.elsevier.com
Consult the Elsevier homepage for full catalogue information on all books, major reference works, journals, electronic products and services.

Elsevier Titles of Related Interest

AN END TO GLOBAL WARMING
L.O. Williams
ISBN: 0-08-044045-2, 2002

FUNDAMENTALS AND TECHNOLOGY OF COMBUSTION
F. El-Mahallawy, S. El-Din Habik
ISBN: 0-08-044106-8, 2002

GREENHOUSE GAS CONTROL TECHNOLOGIES: 6TH INTERNATIONAL CONFERENCE
John Gale, Yoichi Kaya
ISBN: 0-08-044276-5, 2003

MITIGATING CLIMATE CHANGE: FLEXIBILITY MECHANISMS
T. Jackson
ISBN: 0-08-044092-4, 2001

Related Journals:
Elsevier publishes a wide-ranging portfolio of high quality research journals, encompassing the energy policy, environmental, and renewable energy fields. A sample journal issue is available online by visiting the Elsevier web site (details at the top of this page). Leading titles include:

Energy Policy
Renewable Energy
Energy Conversion and Management
Biomass & Bioenergy
Environmental Science & Policy
Global and Planetary Change
Atmospheric Environment
Chemosphere – Global Change Science
Fuel, Combustion & Flame
Fuel Processing Technology

All journals are available online via ScienceDirect: www.sciencedirect.com

To Contact the Publisher
Elsevier welcomes enquiries concerning publishing proposals: books, journal special issues, conference proceedings, etc. All formats and media can be considered. Should you have a publishing proposal you wish to discuss, please contact, without obligation, the publisher responsible for Elsevier's Energy program:

Henri van Dorssen
Publisher
Elsevier Ltd
The Boulevard, Langford Lane
Kidlington, Oxford
OX5 1GB, UK

Phone: +44 1865 84 3682
Fax: +44 1865 84 3931
E.mail: h.dorssen@elsevier.com

General enquiries, including placing orders, should be directed to Elsevier's Regional Sales Offices – please access the Elsevier homepage for full contact details (homepage details at the top of this page).

Carbon Dioxide Capture for Storage in Deep Geologic Formations – Results from the CO_2 Capture Project

Geologic Storage of Carbon Dioxide with Monitoring and Verification

Edited by

Sally M. Benson
Lawrence Berkeley Laboratory
Berkeley, CA,USA

and Associate Editors

Curt Oldenburg[1], Mike Hoversten[1] and Scott Imbus[2]
[1]Lawrence Berkeley National Laboratory
Berkeley, CA, USA
[2]Chevron Texaco Energy Technology Company
Bellaive, TX, USA

Volume 2

ELSEVIER
2005

Amsterdam – Boston – Heidelberg – London – New York – Oxford
Paris – San Diego – San Francisco – Singapore – Sydney – Tokyo

ELSEVIER B.V.
Radarweg 29
P.O. Box 211, 1000 AE Amsterdam
The Netherlands

ELSEVIER Inc.
525 B Street, Suite 1900
San Diego, CA 92101-4495
USA

ELSEVIER Ltd
The Boulevard, Langford Lane
Kidlington, Oxford OX5 1GB
UK

ELSEVIER Ltd
84 Theobalds Road
London WC1X 8RR
UK

First edition 2005

Library of Congress Cataloging in Publication Data
A catalog record is available from the Library of Congress.

British Library Cataloguing in Publication Data
A catalogue record is available from the British Library.

ISBN: 0-08-044570-5 (2 volume set)

Volume 1: Chapters 8, 9, 13, 14, 16, 17, 18, 24 and 32 were written with support of the U.S. Department of Energy under Contract No. DE-FC26-01NT41145. The Government reserves for itself and others acting on its behalf a royalty-free, non-exclusive, irrevocable, worldwide license for Governmental purposes to publish, distribute, translate, duplicate, exhibit and perform these copyrighted papers. EU co-funded work appears in chapters 19, 20, 21, 22, 23, 33, 34, 35, 36 and 37. Norwegian Research Council (Klimatek) co-funded work appears in chapters 1, 5, 7, 10, 12, 15 and 32.

Volume 2: The Storage Preface, Storage Integrity Preface, Monitoring and Verification Preface, Risk Assessment Preface and Chapters 1, 4, 6, 8, 13, 17, 18, 19, 20, 21, 22, 23, 24, 25, 26, 27, 28, 29, 30, 31, 32, 33 were written with support of the U.S. Department of Energy under Contract No. DE-FC26-01NT41145. The Government reserves for itself and others acting on its behalf a royalty-free, non-exclusive, irrevocable, worldwide license for Governmental purposes to publish, distribute, translate, duplicate, exhibit and perform these copyrighted papers. Norwegian Research Council (Klimatek) co-funded work appears in chapters 9, 15 and 16.

♾ The paper used in this publication meets the requirements of ANSI/NISO Z39.48-1992 (Permanence of Paper).
Printed in The Netherlands.

Carbon Dioxide Capture for Storage in Deep Geologic Formations, Volume 2
D.C. Thomas and S.M. Benson (Eds.)

Chapter 13

SIMULATING CO_2 STORAGE IN DEEP SALINE AQUIFERS

Ajitabh Kumar, Myeong H. Noh, Gary A. Pope, Kamy Sepehrnoori, Steven L. Bryant and Larry W. Lake

University of Texas, Austin, TX, USA

ABSTRACT

We present the results of compositional reservoir simulation of a prototypical CO_2 storage project in a deep saline aquifer. The objective was to better understand and quantify estimates of the most important CO_2 storage mechanisms under realistic physical conditions. Simulations of a few decades of CO_2 injection followed by $10^3 - 10^5$ years of natural gradient flow were done. The impact of several parameters was studied, including average permeability, the ratio of vertical to horizontal permeability, residual gas saturation, salinity, temperature, aquifer dip angle, permeability heterogeneity and mineralization. The storage of CO_2 in residual gas emerges as a potentially very significant issue meriting further study. Under some circumstances this form of immobile storage can be larger than storage in brine and minerals.

INTRODUCTION

Geological Storage

Geological storage of CO_2 is one of the few ways to remove combustion emissions in sufficient volumes [1] to mitigate the greenhouse effect. Several groups have reported aquifer-scale simulations of the storage process, usually in order to estimate the volume that can be stored [1–14]. Most schemes that have been put forward depend on storing CO_2 in the supercritical state. In these schemes, buoyancy forces will drive the injected CO_2 upward in the aquifer until a geological seal is reached. The permanence of this type of storage depends entirely on the integrity of the seal over very long periods of time. Assuring such integrity in advance is very difficult.

Our study focuses on three modes of CO_2 storage that avoid this concern: (1) pore-level trapping of the CO_2-rich gas phase within the geologic formation; (2) dissolution into brine in the aquifer; and (3) precipitation of dissolved CO_2 as a mineral, e.g. calcite. All three modes are familiar, though to date not much attention has been paid to the first in the context of CO_2 trapping mechanisms. Each of these modes is permanent for the time frame of interest in CO_2 storage. The key issues then become (1) how to maximize these three highly desirable forms of storage so that very large volumes of CO_2 can be permanently stored in aquifers, without the need for ensuring long-term seal integrity and (2) how long it takes for the injected CO_2 to migrate into these modes of storage.

The principal petrophysical parameters influencing storage as an immobile gas phase (in this chapter, we use the term "gas" as shorthand for "supercritical fluid") are relative permeability, including hysteresis, and the residual saturation of a nonwetting phase. Both depend on the rock making up the aquifer and thus can vary with location. The phase behavior of the CO_2/brine mixture controls storage in solution, and this depends upon brine salinity, temperature, and pressure. The principal geochemical driver accompanying storage is the acidification of the brine resulting from dissociation of dissolved CO_2. Low pH brine 10 in turn induces several reactions with minerals in the formation. An obvious example is the dissolution of carbonate cements. Other reactions are analogous to weathering, in which the acid extracts cations from aluminosilicates (feldspars, clays, etc.). The released cations may form relatively insoluble carbonate precipitates such as siderite. The competition between these reactions will determine the potential for additional storage by mineralization.

The time scales for these processes vary widely. Once CO_2 injection ends, the fluid displacement leading to residual saturations depends on absolute and relative permeabilities, hysteresis, buoyancy forces, the potential gradient caused by dip of the formation, and the magnitude of the residual saturation. Dissolution of CO_2 into brine is rapid, but the overall rate of mass transfer depends on contact between the phases. This is a complicated function of time, especially after injection stops, controlled by the same parameters as the post-injection fluid displacement. Geochemical reactions (mineral dissolution and precipitation) are typically slow [1,10] though under some conditions the rate may be comparable to other mass transport processes [4,14].

EXPERIMENTAL/STUDY METHODOLOGY

To study these processes, their dependence on aquifer parameters, and their characteristic time scales, we conducted a large set of two- and three-dimensional simulations with fully coupled reactive flow and transport. The Computer Modeling Group's GEM simulator was used in this study [8]. Base case simulations were conducted for aquifer storage times of 1000 years. Some simulations were continued for up to 100,000 years.

Because this is a generic study of CO_2 storage in deep, saline aquifers rather than the study of a specific aquifer, the goal was to select representative characteristics for the aquifer as a base case for a systematic parameter study. This provides insight into the potential for CO_2 storage in forms that have minimal tendency to escape from the aquifer.

The input parameters for the base case simulation are summarized in Table 1. The simulated aquifer is 53,000 ft (16,154.4 m) long, 53,000 ft (16,154.4 m) wide and 1000 ft (304.8 m) thick. Constant pressure wells are used along all boundaries to model an open aquifer, while the injector is in the center of the aquifer. These wells are all at the same pressure, so only gravity-driven flow occurs after CO_2 injection. The relative permeability curves are shown in Figure 1.

Pure supercritical CO_2 is injected into the aquifer for 10 years. The injector is then shut in, and the simulation continues with only density differences driving the flow. Having established the base case, we conducted several simulations to study the effect of the parameters influencing the distribution of CO_2 in the aquifer. These parameters include permeability, the ratio of vertical to horizontal permeability, residual gas saturation, salinity, temperature, and dip. Table 2 summarizes the different runs made. These runs did not include geochemical reactions.

This study assumed no conductive faults and no leaky wellbores in the aquifer. Such features would provide a potential escape route for mobile CO_2-rich gas, but not for CO_2 trapped as a residual phase, dissolved in brine, or precipitated as minerals. They would introduce a critical length scale—distance from injector to the potential leak—that would influence the design of strategies to permanently store CO_2. If the injected CO_2 is transformed into trapped forms before it reaches conductive vertical pathways, then risk of escape is small.

RESULTS AND DISCUSSION

Phase Behavior

The calibration of the fluid property models with experimental data is a very important first step in establishing the input to the simulator for this problem. CO_2 solubility is of obvious importance in evaluating storage in brine. Critical to evaluating the permanence of this mode of storage is the brine density: it increases with CO_2 content, hence brine will sink relative to other fluid phases in the aquifer. Thus, CO_2 solubility, brine density and brine viscosity models were calibrated against experimental data as a function of salinity, temperature, and pressure. The brine density and viscosity also depend on the CO_2 concentration.

We made an extensive literature search to find the best sources of experimental data. Table 3 lists the different sources of solubility data for CO_2 in brine [15–19]. These sources give similar trends over a wide range of temperature and salinity.

TABLE 1
SIMULATION INPUT FOR BASE CASE SIMULATION

Aquifer properties		
Length (m)	16,154.4	
Width (m)	16,154.4	
Thickness (m)	304.8	
Depth at top of formation at injection well (m)	1615.44	
Temperature (°C)	60	
Initial pressure (MPa)	15.6	
Dip (degree)	1	
Salinity (ppm)	100,000	
Dykstra–Parsons coefficient	0.7	
Vertical to horizontal permeability ratio	0.001	
Mean permeability (md)	100	
Horizontal permeabilities of each layer,[a] (md)		
Layers 1–4	89	
Layers 5–8	65	
Layers 9–12	46	
Layers 13–16	30	
Layers 17–20	15	
Layers 21–24	120	
Layers 25–28	165	
Layers 29–32	235	
Layers 33–36	840	
Layers 37–40	370	
Porosity	0.25	
Residual water saturation	0.25	
Residual gas saturation	0.25	
Gas end point relative permeability	1.0	
Water end point relative permeability	0.334	
Grid	$40 \times 40 \times 40$	
Maximum injection pressure (MPa)	22.75	
Maximum injection rate (MMSCM/D)	1.416	
Description of components		
Component	*CO_2*	*H_2O*
Critical pressure (MPa)	7.38	22.06
Critical temperature (°C)	30.98	373.94
Critical volume (l/gmole)	0.094	0.056
Molecular weight (g/gmole)	44.01	18.015
Acentric factor (dimensionless)	0.22394	0.344
Parachor (dimensionless)	78	52

[a] Layer 1 is the top layer.

We tuned the Peng–Robinson equation-of-state [20,21] to fit available experimental data on the solubility of CO_2 in brine and the density of brine [22–28] as a function of CO_2 concentration in the brine, brine salinity, temperature, and pressure. Flash calculations are done in the compositional simulator each time step to calculate the phase behavior of the CO_2 and H_2O mixtures in each grid block as well as the density of both the gas and aqueous phases. The binary interaction parameter between the CO_2 and H_2O was adjusted to fit the CO_2 solubility data and the volume shift parameter for H_2O was adjusted to fit the aqueous phase density. The computed curves for CO_2 solubility as a function

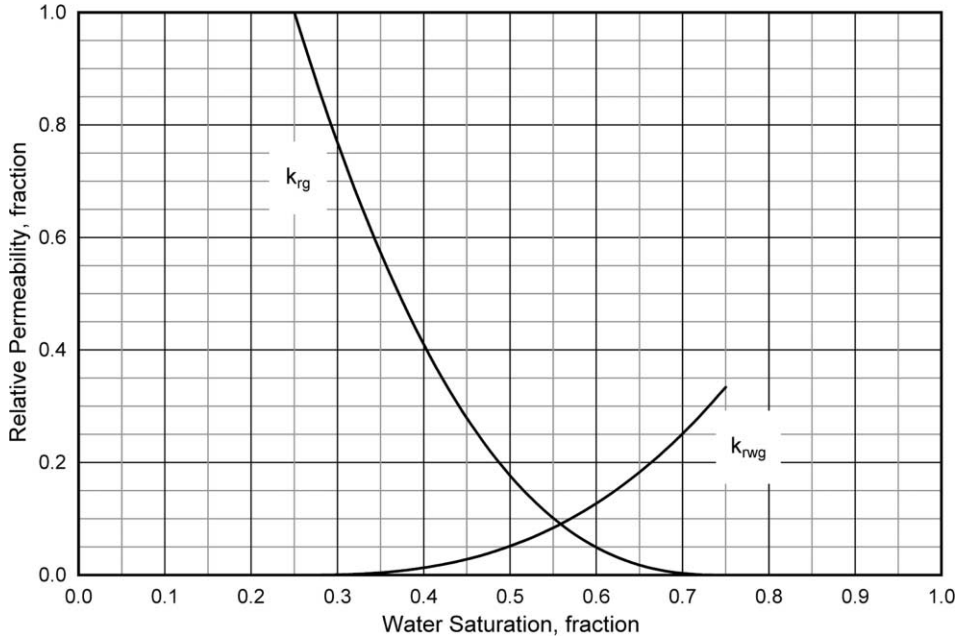

Figure 1: Water–gas relative permeability curves.

TABLE 2
SUMMARY OF SIMULATIONS MADE FOR SENSITIVITY ANALYSIS

Parameter varied	**Results/comments**
Layered permeability—injection for 10 years	
Temperature = 43.33 °C Temperature = 60 °C[a] Temperature = 76.66 °C Temperature = 93.33 °C Temperature = 110 °C	Increase in temperature leads to increased dissolution of gas into brine
Mean permeability = 10 md Mean permeability = 100 md[a] Mean permeability = 1000 md	Increase in mean permeability leads to greater injectivity as well as greater migration of CO_2
Salinity = 0 ppm Salinity = 50,000 ppm Salinity = 100,000 ppm[a] Salinity = 200,000 ppm Salinity = 300,000 ppm	Increase in salinity leads to decreased dissolution of gas into brine

(*continued*)

TABLE 2
CONTINUED

Parameter varied	Results/comments
$k_v/k_h = 0$ $k_v/k_h = 0.001$[a] $k_v/k_h = 0.01$ $k_v/k_h = 0.1$ $k_v/k_h = 1$	Increase in k_v/k_h value leads to upward migration of gas and finally its migration along seal
$S_{gr} = 0.05$ $S_{gr} = 0.15$ $S_{gr} = 0.25$[a] $S_{gr} = 0.35$ $S_{gr} = 0.5$	Low value for S_{gr} leads to increased gas migration and dissolution in brine, while high value leads to increased trapping as residual gas
Dip = 0° Dip = 1°[a] Dip = 2.5° Dip = 5°	Increase in dip leads to increased gas migration and dissolution into brine
Stochastic permeability—injection for 50 years (correlation lengths: $\Delta x = \Delta y = 127, \text{m}$, $\Delta z = 1.27, \text{m}$)	
Mean permeability = 10 md (other properties correlated)	Increase in mean permeability leads to increased injectivity and dissolution into brine
Mean permeability = 1000 md (other properties correlated)	

[a] Base case.

of salinity and pressure are shown in Figure 2 along with selected experimental data points. Similar agreement occurred at temperatures ranging from 68 to 212 °F (20–100 °C). Using the available solubility data, the binary interaction coefficient was correlated linearly with temperature and salinity for a temperature range of 68–212 °F and salinity range of 0–350,000 ppm of NaCl. We tuned the Pedersen correlation for brine viscosity [27].

Density data for pure water was taken from Ref. [26]. This source was preferred because it is based on the IAPWS-95 formulation adopted by International Association for the Properties of Water and

TABLE 3
EXPERIMENTAL DATA FOR CO_2-SOLUBILITY IN BRINE

Source	Temperature range (°C)	Pressure range (MPa)	Salinity range (ppm total dissolved solids)
15	40–160	0.69–9.65	230,000–350,000
16	48.9–150	10–40	0
17	20–100	0.1–60	0
18–19	4.85–19.85	930–4280	0–31,000

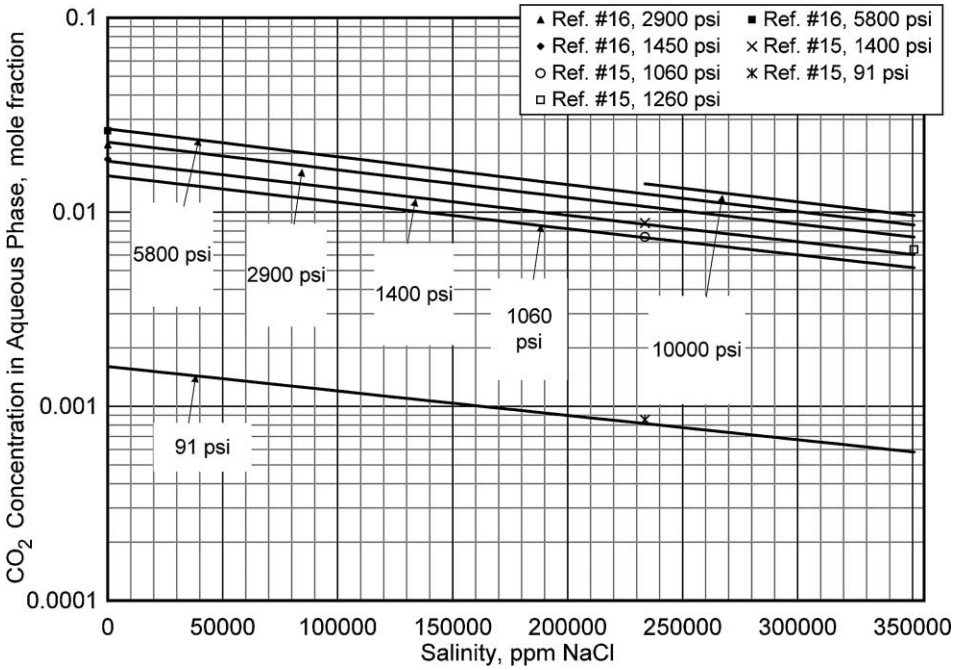

Figure 2: Effect of brine salinity on CO_2 solubility in the aqueous phase at 140 °F (60 °C).

Steam (IAPWS). Density data for pure brine have been taken from Ref. [25] for a wide range of temperature (77–477 °F), pressure (1030–5830 psi), and salinity (30,000–300,000 ppm of NaCl). Unfortunately, there are very few experimental data in the temperature and pressure range of interest for the density of brine saturated with CO_2. Parkinson and Nevers [28] give density values for CO_2–H_2O mixtures for pressures less than 500 psia and temperatures less than 105 °F (40.5 °C). Teng et al. [18,19] give density values of CO_2–brine mixtures for temperatures less than 68 °F (20 °C). Data from Ref. [24] were used to verify density trends. Those few density data that could be found were used to develop a correlation for the volume shift parameter of H_2O used in the Peng–Robinson EOS over the same range of temperature and salinity. Figure 3 shows an example of the predicted density of both brine and brine saturated with CO_2 as a function of salinity at 140 °F (60 °C) and 5830 psia (40.2 MPa). The density of brine saturated with CO_2 is slightly greater than that of brine without CO_2. However, the differences decrease as salinity increases.

Effect of Aquifer Properties

Table 2 summarizes the results when a wide range of aquifer properties were varied individually. Less CO_2 is stored in the 10-year injection period when the formation permeability is small. This is because the simulation includes a maximum bottom hole pressure for the injector, which limits its injection rate.

The effects of temperature and salinity reported in Table 2 reflect the changes in CO_2 solubility and in density of CO_2-saturated brine. The solubility of CO_2 in brine and the viscosity of brine both decrease with an increase in temperature. The former tends to lessen dissolution of CO_2 in brine, while latter increases the same due to increased contact of injected CO_2 with brine. The second phenomenon is more prominent hence at higher temperatures a greater percentage of injected CO_2 goes into aqueous phase. Similarly smaller salinity corresponds to more dissolution because of increased solubility. Larger values for dip lead to greater

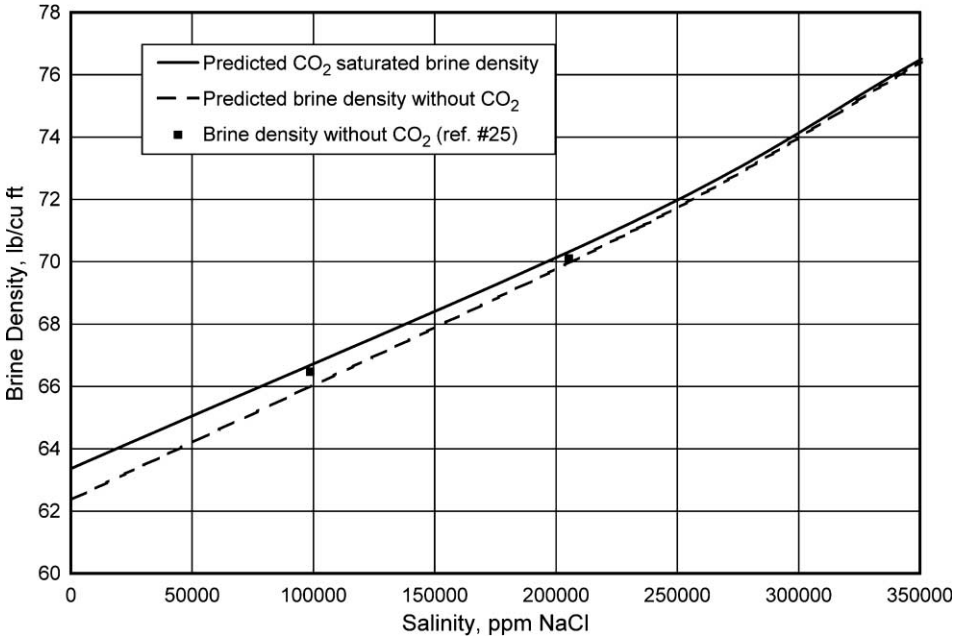

Figure 3: Effect of CO_2 on brine density at 122 °F and 5830 psi.

lateral movement of CO_2, which in turn leads to increased dissolution. Although the vertical to horizontal permeability ratio (k_v/k_h) does not affect the distribution of CO_2 among phases significantly, it does affect spatial distribution. At small values of k_v/k_h, there is more horizontal movement of the CO_2 in the layers into which injection occurred. At larger values, there is more vertical migration followed by movement along the top seal.

Residual gas saturation has the greatest effect on the distribution of CO_2 among the three modes of storage (Figure 4). For small values of residual gas saturation, nearly 20% of the CO_2 is still mobile after 1000 years. Thus, there is greater movement of the CO_2-rich gas phase in the post-injection period. This increases the extent of contact between CO_2 and brine, which in turn leads to increased dissolution of CO_2 in brine. On the other hand, this also permits migration of CO_2 to the top seal of the aquifer. As illustrated later, it also leads to considerable migration along the top of the aquifer in the up-dip direction. In contrast, at larger values of residual gas saturation, most of the CO_2 is trapped as residual gas. There is correspondingly less CO_2 dissolved in brine. Most importantly, the amount of CO_2 that is still mobile after 1000 years is very small.

The strong influence of residual gas saturation on CO_2 storage in aquifers is one of the most important findings of this study. The simulations discussed above assume a single value of residual gas saturation for the entire aquifer. In general, this parameter will vary with rock type [29]. For example, data suggest a correlation between residual gas saturation and porosity [30]. To examine the implications of this variability, we conducted a second set of simulations with stochastic porosity/permeability realizations (Table 2). The porosity values for each block were then calculated using the following correlation [30].

$$\phi = \left(\frac{k}{7\times 10^7}\right)^{1/9.606}$$

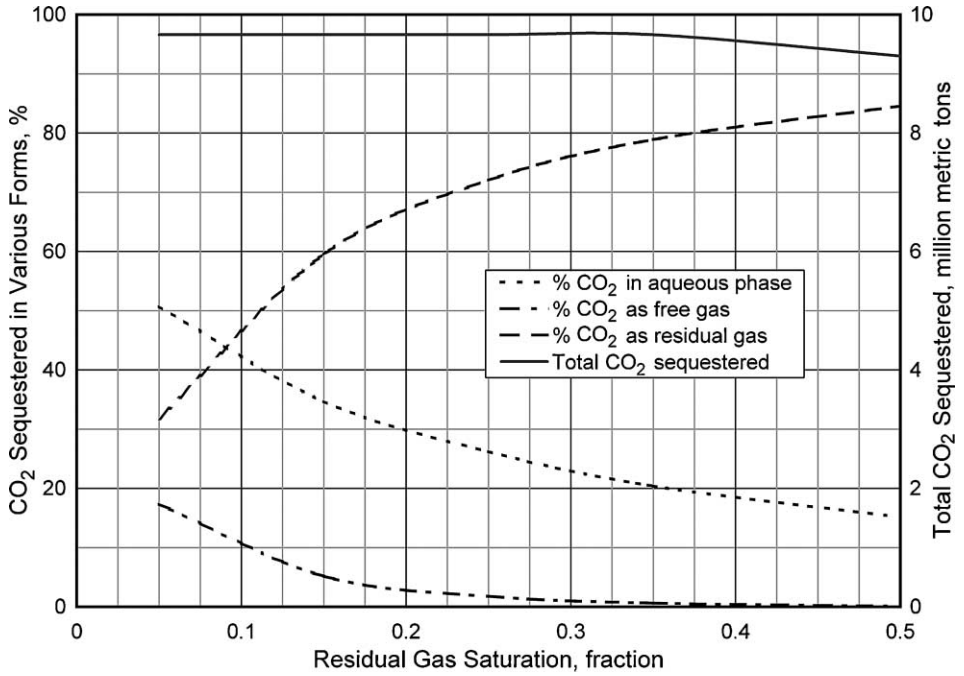

Figure 4: Effect of residual gas saturation on the distribution of CO_2 between phases at 1000 years.

Based on the values of porosity for each grid, maximum residual gas saturation and residual water saturation values were found using following correlations [30].

$$S_{gr}^{max} = 0.5473 - 0.9696\phi; \qquad S_{wirr} = 5.6709 \times (\mathrm{Log}(k)/\phi)^{-1.6349}$$

We also accounted for the fact that the relative permeability of the gas phase depends on whether it is displacing or being displaced by water. GEM models hysteresis with the following equations:

$$k_{rg}(S_g) = k_{rg}(\mathrm{Drainage};\ S_g)\text{during drainage}; \qquad k_{rg}(S_g) = k_{rg}(\mathrm{Drainage};\ S_g(\mathrm{shifted}))\text{during imbibition};$$

where

$$S_g(\mathrm{shifted}) = \frac{(S_g - S_{grh})(S_{gh})}{(S_{gh} - S_{grh})} \qquad \text{and} \qquad \frac{1}{S_{gr}^{max}} - 1 = \frac{1}{S_{grh}} - \frac{1}{S_{gh}}$$

S_{gh} is the value of S_g when the shift to imbibition occurs, S_{grh} is the value of S_{gr} corresponding to S_{gh} via Land's equation, and S_{gr}^{max} has the value of the user-entered parameter S_{gr}^{max}.

In these simulations, a set of 10–15 intervals of porosity values was defined. Each interval was assumed to represent a single rock type and hence was assigned a different relative permeability curve and a different value of S_{gr}^{max} and S_{wirr}. The latter were calculated using the average porosity value for the interval. Figure 5 shows the correlation between different aquifer properties plotted with actual values used in simulations. An example relative permeability curve is shown in Figure 6.

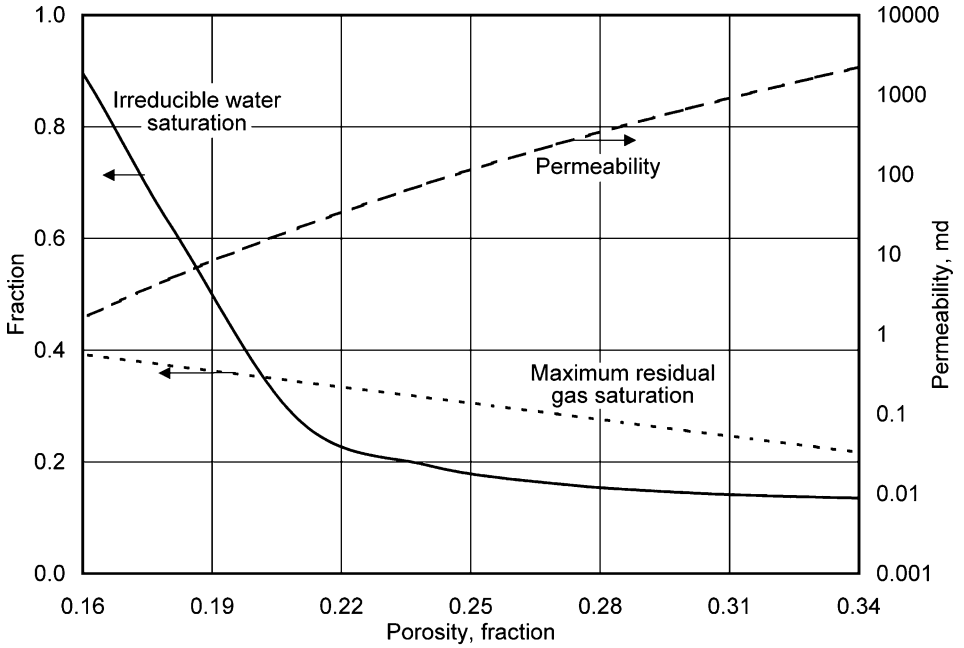

Figure 5: Correlation between different aquifer properties [30].

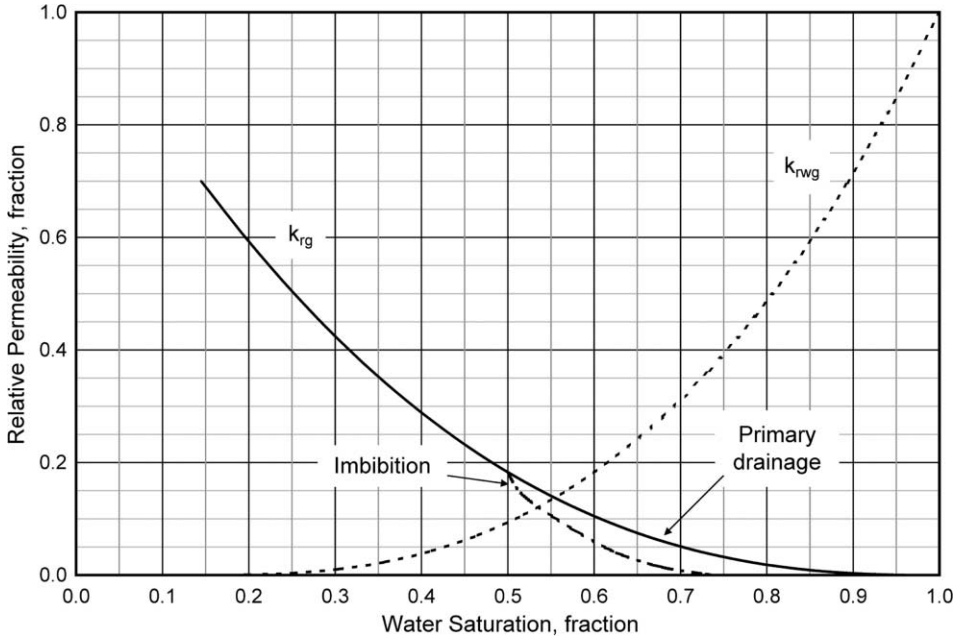

Figure 6: Water–gas relative permeability curves with hysteresis.

To study the effect of the injector completion, CO_2 was injected only in the bottom half of the aquifer. Also, CO_2 was injected for 50 years, rather than 10 years, to investigate how the much larger volume of CO_2 would affect storage.

The simulations conducted with partial well completion in stochastic porosity/permeability realizations with hysteretic relative permeability and rock-type-dependent residual gas saturation indicate that with time all the gas will be trapped in various forms and will never reach the top seal of the aquifer. Figure 7 shows the gas injection profile at 50 years for a vertical $x-z$ cross-section through the injector. Figure 8 shows the same profile after 1000 years. Figure 9 shows the CO_2 mole fraction in the aqueous phase for the same cross-section after 1000 years.

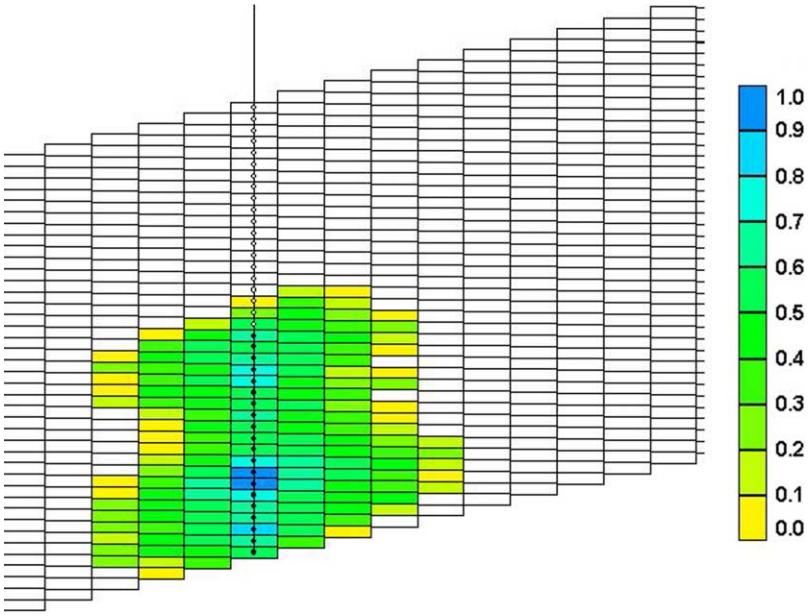

Figure 7: Gas saturation at 50 years (zoomed-in vertical slice through the injection well in $x-z$ direction).

Some 25% of the injected CO_2 exists as a mobile CO_2-rich gas phase at the end of the 50-year injection period. Figure 10 shows an important consequence of buoyancy-driven fluid movement after injection ends: CO_2 is transferred from the mobile phase into permanently stored forms. The time scale for this transfer depends strongly on aquifer properties, including dip; for this example the transfer is essentially complete within 1000 years. This simulation shows the benefit of CO_2 movement after injection ends, but this movement also presents a potential disadvantage. Figure 11 shows the gas saturation profile at 1000 years when CO_2 is injected through the entire interval of the well, rather than the bottom half. Migration of CO_2 up dip along the top seal is evident. This result emphasizes the importance of engineering design in an aquifer storage scheme. A good understanding of the target formation, of the key physicochemical phenomena, and of classical reservoir engineering concepts will be prerequisite for ensuring long-term storage.

Influence of Mineralization

To study the possible contribution of mineralization to CO_2 storage, we performed a third set of simulations in a one-dimensional tilted aquifer (1° dip) derived from the base case described above. This is shown

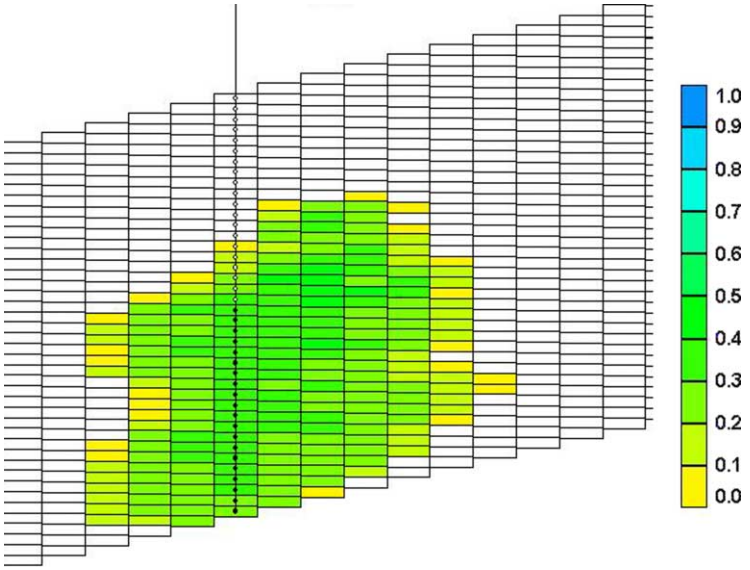

Figure 8: Gas saturation at 1000 years (zoomed-in vertical slice through the injection well in $x-z$ direction).

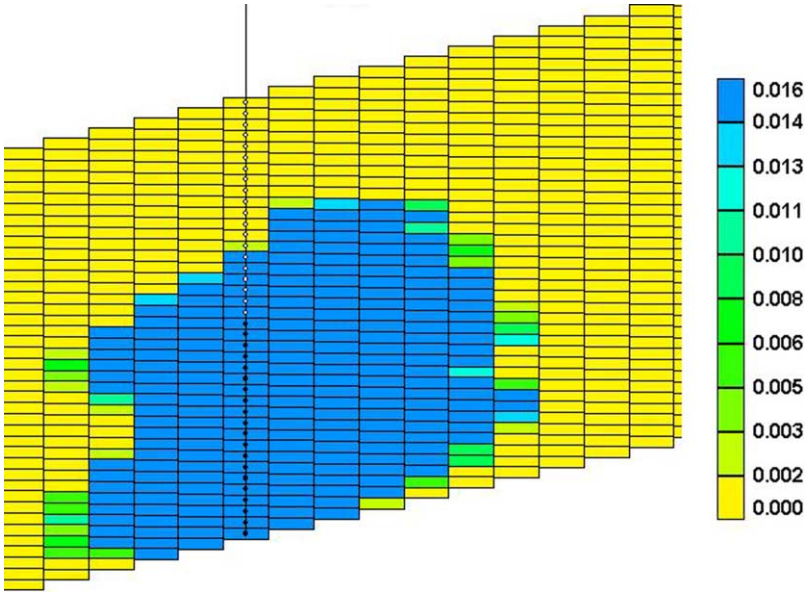

Figure 9: CO_2 mole fraction in aqueous phase at 1000 years (zoomed-in vertical slice through the injection well in $x-z$ direction).

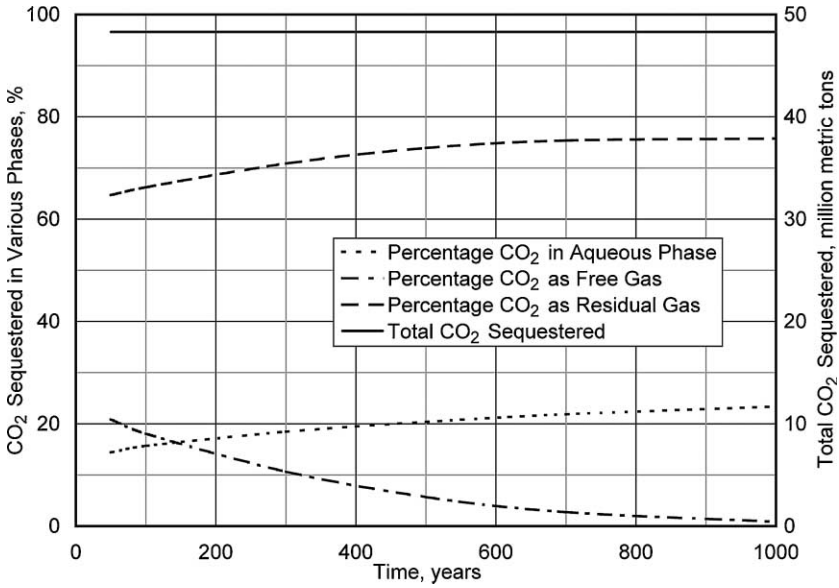

Figure 10: Effect of gravity-driven fluid migration on the distribution of CO_2 between phases after injection for 50 years (at 1000 years).

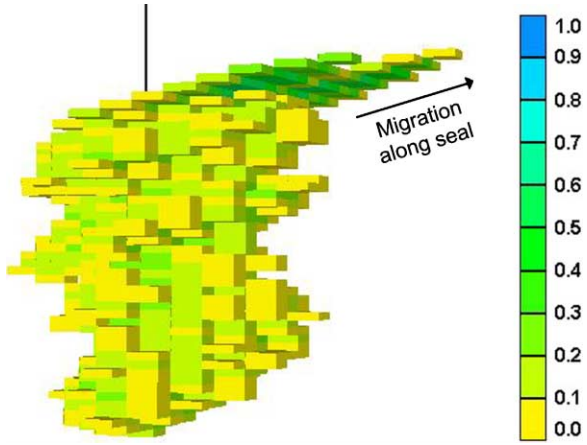

Figure 11: 3D gas saturation profile at 1000 years for injection along whole interval.

schematically in Figure 12. The homogeneous horizontal permeability is 197.5 md and the porosity is 0.25. The reservoir temperature is 60 °C and the diffusion coefficient is 2×10^{-5} cm^2/s. Salinity is 100,000 ppm. For simplicity, CO_2 solubility was modeled with Henry's law [8,20], using a constant of 3.85×10^5 kPa. Relative permeability curves are shown in Figure 1 and capillary pressure is ignored.

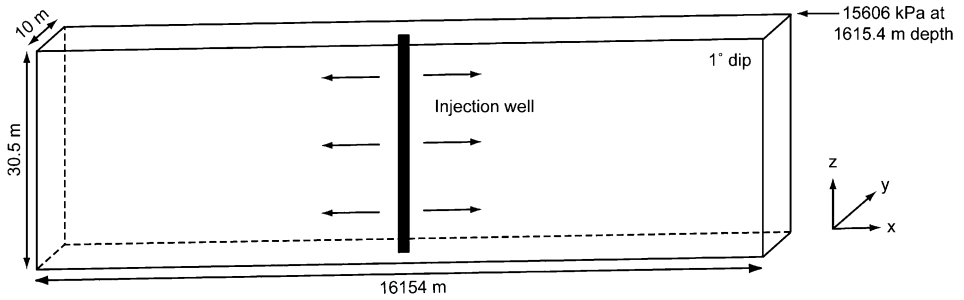

Figure 12: Schematic of 1D flow field used for simulations that account for mineralization.

The three aqueous reactions and five mineral reactions, described in Tables 4 and 5, were used in all simulations. The mineral properties and compositions are based on a glauconitic sandstone aquifer in the Alberta Sedimentary Basin, Canada [4–8]. The reaction equations for the five minerals are as follows:

$$\text{Calcite} + H^+ \leftrightarrow Ca^{2+} + HCO_3^-$$

$$\text{Anorthite} + 8H^+ \leftrightarrow 4H_2O + Ca^{2+} + 2Al^{3+} + 2SiO_2(aq)$$

$$\text{Kaolinite} + 6H^+ \leftrightarrow 5H_2O + 2SiO_2(aq) + 2Al^{3+}$$

$$\text{Siderite} \leftrightarrow Fe^{2+} + CO_3^{2-}$$

$$\text{Glauconite} + 14H^+ \leftrightarrow 1.5K^+ + 2.5Fe^{3+} + 0.5Fe^{2+} + Mg^{2+} + Al^{3+} + 7.5SiO_2(aq) + 9H_2O$$

TABLE 4
AQUEOUS REACTIONS

Reaction	**Equilibrium constant, $\log_{10} K$**
$H_2O \leftrightarrow H^+ + OH^-$	−13.2631
$CO_2(aq) + H_2O \leftrightarrow H^+ + HCO_3^-$	−6.3221
$CO_2(aq) + H_2O \leftrightarrow 2H^+ + CO_3^{2-}$	−16.5563

TABLE 5
MINERAL REACTIONS

Mineral	**$\text{Log}_{10} K_{sp}$**	**$\text{Log}_{10} k_\beta$ (mole/m^2 s)**	**$\hat{A}_\beta$ (m^2/m^3)**	**Ea_β (J/mole)**
Calcite	1.36	−8.8	88	41,870
Anorthite	−8	−12	88	67,830
Kaolinite	5.47	−13	17,600	62,760
Siderite	10.7	−9.35	88	41,870
Glauconite	−8.6	−14	4400	58,620

Table 6 shows the initial concentrations for aqueous components and the mineral properties and initial volume fractions are shown in Table 7. In this example, we set the residual gas saturation to 0.25 and the initial gas saturation to be zero. Supercritical CO_2 is injected for 10 years with the rate of 100 m^3/day. A production

TABLE 6
INITIAL CONCENTRATIONS FOR AQUEOUS COMPONENTS

Aqueous species	Concentration, mole/g H_2O
$H+$	1.0×10^{-10}
Ca^{2+}	9.12×10^{-8}
SiO_2(aq)	2.35×10^{-11}
Al^{3+}	2.32×10^{-14}
Fe^{2+}	3.22×10^{-9}
Fe^{3+}	4.99×10^{-8}
Mg^{2+}	5×10^{-10}
K^{+}	5×10^{-10}
OH^{-}	5.46×10^{-10}
CO_3^{2-}	2.49×10^{-5}
HCO_3^{-}	1.17×10^{-8}

TABLE 7
MINERAL PROPERTIES

Mineral	Molecular weight	Density (g/m^3)	Initial volume fraction
Calcite	100.1	2.71	0.0088
Anorthite	278.2	2.74	0.0088
Kaolinite	258.16	2.41	0.0176
Siderite	115.86	3.96	0.0088
Glauconite	426.93	2.67	0.044

well is placed at each boundary to maintain constant far-field pressure. The total amount of CO_2 injection is 9.2×10^9 gmole. Then we stop the CO_2 injection and continue the simulation for 10,000 years.

The average abundances of calcite and siderite for case 1 are shown in Figure 13. During the CO_2 injection period, the calcite initially present in the aquifer starts to dissolve because the dissolved CO_2 perturbs the initial aqueous phase composition so that it becomes undersaturated with respect to calcite. Since the average water saturation decreases during the first 10 years, mineral abundances increase even though mineral dissolution occurs. Figure 13 shows that the mineralization (precipitation of calcite) starts after the injection stops. The siderite curve does not show significant responses after 10 years.

Anorthite and calcite average abundances are presented on a linear time axis in Figure 14. The calcite abundance increases nonlinearly and stabilizes at 1.62×10^3 gmole/kg water. Calcite precipitation requires a source of calcium cations, which provided in this example by the dissolution of anorthite. Thus, the calcite precipitation is symmetric with the anorthite dissolution. Because very little fluid migration occurs after injection ends, the perturbation of the aqueous phase composition is limited to the region contacted by CO_2 during injection. This defines the mineralization region. The anorthite abundance in Figure 14 becomes constant when most of the anorthite in the mineralized region has dissolved, after 10,000 years. In this example, 90.8% of injected CO_2 remains as a gas phase and 6.4% dissolves into water. About 2.7% of the CO_2 is mineralized into calcite. A relatively small amount of CO_2 stays as the bicarbonate ion (HCO_3^-) and the amounts of the siderite precipitation and the carbonate ion are negligible. Even though the residual gas saturation is a modest 0.25, the residual saturation trapping is 46.8 and 44% of total CO_2 is still mobile.

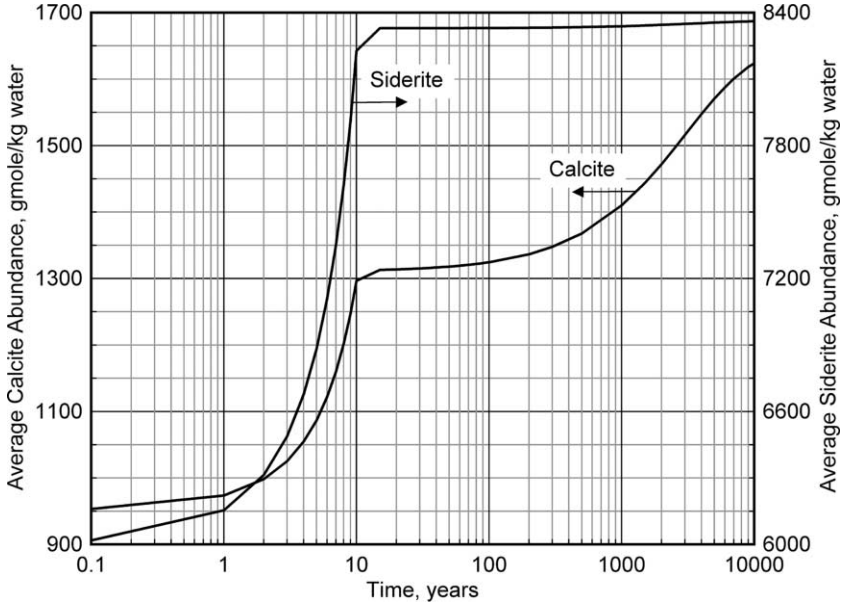

Figure 13: Mineral abundances for case 1.

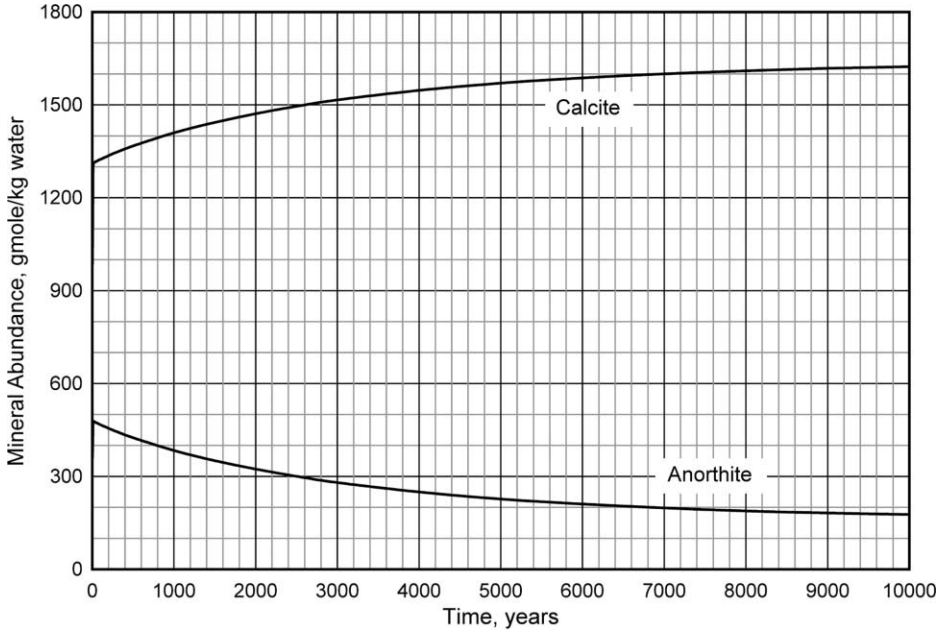

Figure 14: Abundance history of anorthite and calcite for case 1.

In the case described above (case 1), we consider only CO_2 injection, and the majority of CO_2 remains in the gas phase. To evaluate the potential for reducing the amount of mobile gas in the aquifer, we simulated the injection of water simultaneously with the CO_2 injection (case 2). We also simulated the injection of the same amount of the water as in case 2, but immediately after the CO_2 injection (case 3). As was mentioned previously, mineral precipitation depends highly on the amount and type of the source minerals, e.g. the anorthite dissolution as a precursor for calcite precipitation. If we inject CO_2 in an anorthite-rich aquifer (case 4), more calcite precipitation will occur. In case 4, we increase the initial volume fraction of anorthite to 0.088, which is 10 times larger than case 3, and the sequential water injection is also applied. Table 8 summarizes the formulation of simulation runs. The injection of water causes the gas saturation to decrease in the region around the injector because the CO_2 is displaced, and because the CO_2 remaining dissolves into water. Saturation fronts for cases 1 and 2 are the same because the same amount of CO_2 is injected for 10 years for both cases. When CO_2 and water are injected sequentially, water pushes the gas saturation front and there is less mobile gas than the simultaneous injection case because CO_2 has more contact with the formation water. Only 10% of injected CO_2 remains mobile after 10,000 years in case 3.

TABLE 8
SUMMARY OF SIMULATIONS WITH MINERAL REACTIONS

Case 1: CO_2 injection only	Injection 100 m^3/day of CO_2 for 10 years and shut-in
Case 2: simultaneous water injection	Co-injection 100 m^3/day of CO_2 and 100 m^3/day of water for 10 years and shut-in
Case 3: sequential water injection	Sequential injection 100 m^3/day of CO_2 for 10 years, then 100 m^3/day of water for another 10 years and shut-in
Case 4	Increase initial anorthite abundance to 10 times more than that of case 3

Table 9 presents the CO_2 storage in various forms for each case at 10,000 years. Forty-four percent of injected CO_2 remains as a mobile gas phase in case 1. Compared with Figure 4, as 1D test cases ignore the buoyancy of the gas phase so more injected CO_2 remains as mobile gas when compared to the 3D cases. Even though the same amount of water is injected for cases 2 and 3, more CO_2 dissolves into water when we apply the water injection sequentially. Owing to the large solubility of CO_2 in water, the injected water will dissolve out the residual gas phase saturation.

TABLE 9
DISTRIBUTION [%] OF INJECTED CO_2 FOR TEST CASES AT 10,000 YEARS

	Gas		**Aqueous**	**HCO_3^-**	**Calcite**
	Mobile	**Immobile**			
Case 1	44.0	46.8	6.4	0.1	2.7
Case 2	31.9	55.2	9.4	0.1	3.4
Case 3	10.0	70.6	14.7	0.2	4.5
Case 4 (70,000 years)	2.7	43.3	10.3	0.1	43.6

Figure 15 compares the calcite precipitation between case 3 and 4. In case 4, the calcite precipitation occupies 43.6% of CO_2 for 70,000 years and keeps increasing thereafter. Compared with case 3, about 22% of CO_2 in gas phase is precipitated as calcite and the CO_2 dissolution in the aqueous phase is slightly decreased. If all the anorthite in the aquifer were converted to calcite, the theoretical potential of mineral trapping would be 46.2% of the injected CO_2.

Figure 15 shows that mineralization is negligible over the time scales considered in Figures 7–9, i.e. over the span of 1000 years. The fraction of injected CO_2 stored as calcite begins to increase after a few thousand years. The transfer of CO_2 from the gas phase to the mineral phase (mediated by the aqueous phase dissolution of anorthite) is limited by the rate of anorthite dissolution. Given enough time and a sufficient supply of calcium ion, however, this mechanism substantially decreases the amount of CO_2 stored as a mobile gas phase.

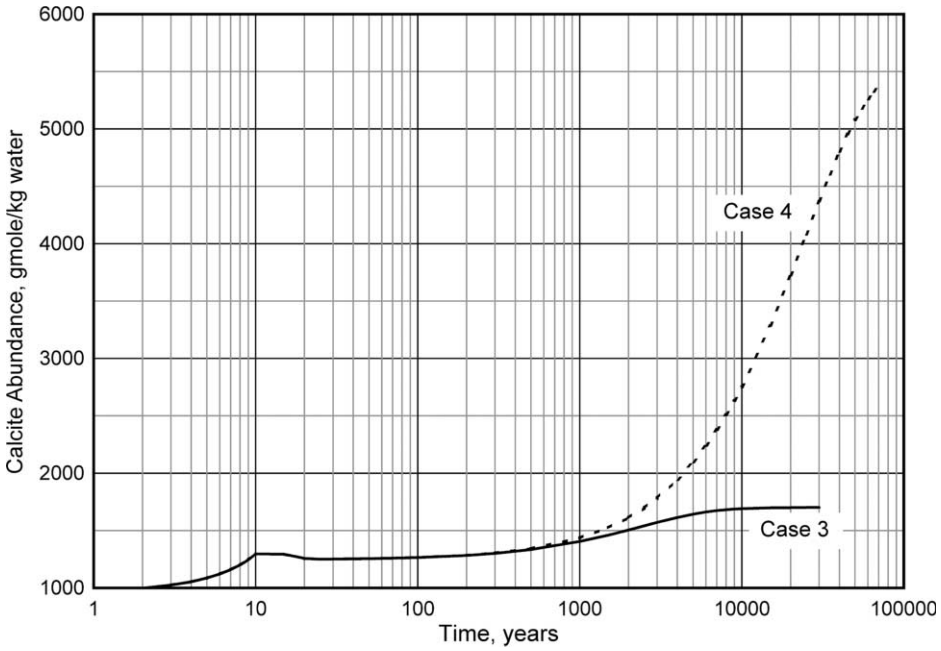

Figure 15: Comparison of calcite precipitation histories for cases 3 and 4. Case 4 has 10 times more initial anorthite than case 3.

CONCLUSIONS

The concerns about CO_2 escape pathways from aquifers used for storage can be considerably mitigated if all or almost all of the CO_2 were stored in the immobile forms of residual gas, dense brine, and minerals. We simulated CO_2 injection in deep, saline aquifers with emphasis on those mechanisms that would immobilize (store) the CO_2. The most significant conclusion from this scoping study is that the effect of residual gas on CO_2 storage can be very large, even more significant than storage in brine or minerals. Potentially all of the CO_2 can be stored in an immobile form when advantage is taken of this well-known phenomenon of capillary trapping. Therefore, the magnitude and variation of residual gas saturation as a petrophysical property merit further study. Both aquifer dip and vertical to horizontal permeability

ratio have a significant effect on gas migration, which in turn affects CO_2 dissolution in brine and mineralization.

Well completions play an important role in deciding the fate of CO_2 after injection. When the supercritical CO_2 enters the aquifer near the top seal, it is likely to continue to migrate up dip for long distances and thus may eventually find an escape path. In contrast, when the CO_2 is injected in the bottom half of the aquifer, gravity-driven flow steadily reduces the amount of mobile gas before it can migrate to the top of the aquifer. The time scale for reduction of mobile gas to insignificant values strongly depends on the petrophysical parameters of the aquifer. Over the range of parameters investigated in this scoping study, very little mobile gas remained in the aquifer after a few hundred years.

For the cases studied, mineralization (conversion of dissolved CO_2 into carbonate minerals) occurs over a much longer time scale, on the order of 10^4 years, primarily because of the slow reaction rates of the chemical reactions. However, if the rate of gravity-driven gas movement is sufficiently small, mineralization could play a significant role in immobilizing injected CO_2.

Injecting water after the CO_2 injection period increases the storage capacities of solubility and mineral trapping. The amount of the mobile gas phase drops significantly because the gas phase is displaced by the injected water and spreads out. This effect would be attenuated if the injected water were saturated with CO_2.

For the cases studied here, the capacity of CO_2 storage by mineral trapping is relatively small compared to residual saturation trapping or mobile gas. The amount of minerals containing divalent cations initially present in the aquifer, and the rate at which they dissolve, control the relative amounts of carbonate minerals precipitated.

RECOMMENDATIONS

1. As study shows, significant amount of injected CO_2 (around 75%) remains as trapped gas at the end of 1000 years, hence it is important to model residual gas saturation correctly.
2. The possibility that mobile CO_2-rich gas could reach conductive fractures/faults before becoming trapped should be studied in more detail for any particular formation.
3. Accurate estimation of dip and vertical to horizontal permeability ratio would help predict the extent of gas migration.
4. Proper well completion may significantly reduce chances of CO_2 leakage. This may obviate the need for a “perfect” seal at the top of the formation.

NOMENCLATURE

k permeability, md
k_{rg} gas relative permeability
k_{rw} water relative permeability
S_g gas saturation, fraction
S_{gr}^{max} maximum residual gas saturation, fraction
S_{wirr} irreducible water saturation, fraction

Greek Symbols
ϕ porosity

ACKNOWLEDGEMENTS

This research was supported by fellowships and grants from the National Energy Technology Laboratory of the U.S. Department of Energy and the CO_2 Capture Program. We especially wish to thank Duane Smith at

NETL for his support of the initial CO_2 research by Vikas and A. Kumar at UT as part of their MS theses. We also want to thank CMG Ltd. for making available the GEM simulator used in this research. Larry W. Lake holds the W. A. (Monty) Moncrief Centennial Chair, Kamy Sepehrnoori holds the Bank of America Centennial Professorship, and Gary A. Pope holds the Texaco Centennial Chair at The University of Texas at Austin.

REFERENCES

1. K. Pruess, T. Xu, J. Apps, J. Garcia, Numerical modeling of aquifer disposal of CO_2, *SPE J., SPE 83695* (2003) 49–60. March.
2. S. Bachu, W.D. Gunter, E.H. Perkins, Aquifer disposal of CO_2: hydrodynamic and mineral trapping, *Energy Convers. Manage.* **35** (1994) 269–279.
3. C. Doughty, K. Pruess, Modeling supercritical CO_2 injection in heterogeneous porous media, *Paper Presented at TOUGH Symposium*, California, May 2003.
4. W.D. Gunter, B. Wiwchar, E.H. Perkins, Aquifer disposal of CO_2-rich greenhouse gases: extension of the time scale of experiment for CO_2-storing reactions by geochemical modeling, *Mineral. Petrol.* **59** (1997) 121–140.
5. B. Hichon, W.D. Gunter, T. Gentzis, The serendipitous association of sedimentary basins and greenhouse gases, *Proceedings, American Chemical Society Symposium on CO_2 Capture*, Utilization and Disposal Orlando, Florida, 1996, pp. 25–29.
6. N.J. House, D.D. Faulder, G.L. Olson, J.R. Fanchi, Simulation study of CO_2 storage in a North Sea Formation, *Paper SPE 81202 Presented at the SPE/EPA/DOE Exploration and Production Environmental Conference*, San Antonio, March 2003.
7. J. Ennis-King, Role of convective mixing in the long-term storage of carbon dioxide in Deep Saline Formations, *Paper SPE 84344 Presented at SPE Annual Technical Conference and Exhibition*, October 2003.
8. L. Nghiem, Compositional Simulator for Carbon Dioxide Storage, Computer Modeling Group Ltd., 2002.
9. S.M. Pasala, C.B. Forster, S.J. Lim, M.D. Deo, Simulating the impact of faults on CO_2 storage and enhanced oil recovery in Sandstone Aquifers, *Paper SPE 84186 Presented at the SPE Annual Technical Conference and Exhibition*, Denver, October 2003.
10. K. Pruess, A. Bielinski, J. Ennis-King, J. Fabriol, Y.L. Gallo, J. García, K. Jessen, T. Kovscek, D.H.S. Law, P. Lichtner, C. Oldenburg, R. Pawar, J. Rutqvist, C. Steefel, B. Travis, C.F. Tsang, S. White, T. Xu, Code Intercomparison Builds Confidence in Numerical Models for Geologic Disposal of CO_2, http://www-esd.lbl.gov/GEOSEQ/index.html.
11. J.G. Seo, D.D. Mamora, Experimental and simulation studies of storage of supercritical carbon dioxide in depleted gas reservoirs, *Paper SPE 81200 Presented at the SPE/EPA/DOE Exploration and Production Environmental Conference*, San Antonio, March 2003.
12. T. Xu, J.A. Apps, K. Pruess, Analysis of Mineral Trapping for CO_2 Disposal in Deep Aquifers, *Report LBNL-46992*, Lawrence Berkeley National Laboratory, Berkeley, CA, 2001.
13. Vikas, Simulation of CO_2 storage, MS thesis, University of Texas at Austin, 2002.
14. T.P. Wellman, R.B. Grigg, B.J. McPherson, R.K. Svec, P.C. Lichtner, Evaluation of CO_2–brine–reservoir rock interaction with laboratory flow tests and reactive transport modeling, Paper SPE 80228 *Presented at the SPE International Symposium on Oilfield Chemistry*, Houston, February 2003.
15. B. Rumpf, H. Nicolaisen, C. Ocal, G. Maurer, Solubility of carbon dioxide in aqueous solutions of sodium chloride: experimental results and correlation, *J. Solution Chem.* **23** (3) (1994) 431–438.
16. P. Scharlin, Carbon Dioxide in Water and Aqueous Electrolyte Solutions, Solubility Data Series, vol. 62, Oxford University Press, *International Union of Pure and Applied Chemistry*, Oxford, 1996.
17. N. Spycher, K. Pruess, J. Ennis-King, CO_2–H_2O Mixtures in the Geological Storage of CO_2. I. Assessment and Calculation of Mutual Solubilities from 12 to 100 °C and up to 600 bar, *Report LBNL-50991*, Lawrence Berkeley National Laboratory, 2002.
18. H. Teng, A. Yamasaki, Solubility of liquid CO_2 in synthetic sea water at temperatures from 278 K to 293 K and pressures from 6.44 MPa to 29.49 MPa, and densities of the corresponding aqueous solutions, *J. Chem. Eng. Data* **43** (1998) 2–5.

19. H. Teng, A. Yamasaki, M.K. Chun, H. Lee, Solubility of liquid CO_2 in water at temperatures from 278 K to 293 K and pressures from 6.44 MPa to 29.49 MPa and densities of the corresponding aqueous solutions, *J. Chem. Eng. Data* **29** (1997) 1301–1310.
20. Y.K. Li, L.X. Nghiem, Phase equilibria of oil, gas and water/brine mixtures from a cubic equation of state and Henry's law, *Can. J. Chem. Eng.* **64** (1986) 486–496.
21. A. Firoozabadi, R. Nutakki, T.W. Wong, K. Aziz, Predictions of compressibility and phase behavior in systems containing water, hydrocarbons, and CO_2, *SPE Reservoir Eng., SPE 15674* **3** (2) (1988).
22. J.E. Garcia, Density of Aqueous Solutions of CO_2, *Report LBNL-49023*, Lawrence Berkeley National Laboratory, 2001.
23. U. Grigull, J. Straub, P. Schiebener, Steam *Tables in SI-Units*, third ed., Springer, Berlin, 1990.
24. L. Hnědkovský, R.H. Wood, V. Majer, Volumes of aqueous solutions of CH_4, CO_2, H_2S and NH_3 at temperatures from 298.15 K to 705 K and pressures to 35 MPa, *J. Chem. Thermodyn.* **28** (1996) 125–142.
25. J.M. Simonson, C.S. Oakes, R.J. Bodnar, Densities of NaCl(aq) to the temperature 523 K at pressures to 40 MPa measured with a new vibrating-tube densitometer, *J. Chem. Thermodyn.* **26** (1994) 345–359.
26. W. Wagner, A. Pruß, The IAPWS formulation 1995 for the thermodynamic properties of ordinary water substance for general and scientific use, *J. Phys. Chem. Ref. Data* **31** (2) (2002) 387–535.
27. I.D. Zaytsev, G.G. Aseyev, Properties of Aqueous Solutions of Electrolytes, CRC Press, Boca Raton, FL, 1992.
28. W. Parkinson, N.D. Nevers, Partial molal volume of carbon dioxide in water solutions, *Ind. Eng. Chem. Fundam.* **8** (4) (1969) 709–713.
29. L.W. Lake, Enhanced Oil Recovery, Prentice-Hall, New Jersey, 1989.
30. H.M. Holtz, Residual gas saturation to aquifer influx: a calculation method for 3-D computer reservoir model construction, *Paper SPE 75502 Presented at SPE Gas Technology Symposium*, April–May 2002.